International Journal of Heat and Fluid Flow 30 (2009) 993–1006

Contents lists available at ScienceDirect

International Journal of Heat and Fluid Flow

journal homepage: www.elsevier.com/locate/ijhff

Near-wall behavior of turbulent wall-bounded flows

Matthias H. Buschmann [a,*], Thomas Indinger [b], Mohamed Gad-el-Hak [c]

[a] Institut für Luft- und Kältetechnik Dresden, Bertolt-Brecht-Allee 20, 01309 Dresden, Germany
[b] Technische Universität München, Institute of Aerodynamics, Boltzmannstr., 15, 85748 Garching, Germany
[c] Virginia Commonwealth University, Richmond, VA 23284-3015, USA

ARTICLE INFO

Article history:
Received 17 November 2008
Received in revised form 26 May 2009
Accepted 4 June 2009
Available online 28 July 2009

Keywords:
Turbulent boundary layer
Shear and normal stresses
Wall-behavior
Peak position

ABSTRACT

A data base compiling a large number of results from direct numerical simulations and physical experiments is used to explore the properties of shear and normal Reynolds stresses very close to the wall of turbulent channel/pipe flows and boundary layers. Three types of scaling are mainly investigated, classical inner, standard mixed, and pure outer scaling. The study focuses on the wall behavior, the location and the value of the peak Reynolds shear stress and the three normal stresses. A primary observation is that all of these parameters show a significant Kármán number dependence. None of the scalings investigated works in an equal manner for all parameters. It is found that the respective first-order Taylor series expansion satisfactorily represents each stress only in a surprisingly thin layer very close to the wall. In some cases, a newly introduced scaling based on $u_\tau^{3/2}u_e^{1/2}$ offers a remedy.

1. Motivation

The near-wall region of a turbulent flow is of special importance for technical applications because the main part of turbulent energy is produced there. Heat and momentum transport, chemical reactions and the viscous drag of a smooth body are strongly influenced by the turbulent motion nearest to the wall. However, numerical simulations used widely in industrial practice insufficiently resolve these near-wall flow phenomena. This is mainly caused by strong flow inhomogenity and directionality close to the wall, which are at best incompletely represented by current turbulence models. At present time, there is an increasing interest in coherent structures affecting near-wall turbulence. Recent experiments (e.g., Adrian, 2007; Hutchins and Marusic, 2007) and theoretical work (e.g., Morrison, 2007; Panton, 2007) show that turbulence structures scaling with different length scales interact in the vicinity of the wall.

Crucial for scaling Reynolds stresses close to the wall is the understanding that wall-parallel u, w and wall-normal v components are affected differently by the solid surface (Morrison et al., 2004). While the former are subjected to the no-slip condition, the latter is diminished by the impermeability constraint. These effects persist even at very high Reynolds numbers, and lead to an entirely different behavior of the fluctuating components. Moreover, as Morrison et al. (2004) have noted, the influence of large scales increase with increasing Reynolds number and with decreasing distance from the wall. In a recent paper, Morrison (2007) identified the local-equilibrium idea—leading to the classical logarithmic law—as a 'no-interaction' condition. In reality, the large eddies near the surface can be understood *as a quasi-inviscid, low-frequency modulation of the shear stress-bearing motion*. Therefore, one may argue that the failure of classical scaling results from neglecting the interaction of near-wall modes that scale on wall-variables with global outer modes scaling on channel height or boundary layer thickness. Jiménez and Hoyas (2008) showed that the intensities of these outer structures do not scale with u_τ and are therefore responsible for the failure of classical scaling in the outer region. All of these arguments make plausible why scaling of near-wall stresses based purely on inner variables seems to be invalid (Buschmann and Gad-el-Hak, 2009a).

Despite the impressive amount of data that was collected in the last 50–60 years, the understanding and especially the modelling of near-wall turbulence make only slow progress. The determination of many flow parameters is difficult or even impossible. The application of invasive experimental techniques (pitot probe, hot-wire, etc.) is problematic due to the interaction of the probes with the wall and their integrating behavior. Results obtained with non-invasive experimental techniques (LD, PIV, etc.) are rare and also do not always provide consistent pictures. Direct numerical simulations (DNS) is a remedy but thus far has been carried out only for relatively low Reynolds numbers and simple geometries. However, recent physical experiments confirm again and again the existence of large and very large structures within the flow having length scales much larger than the integral length scales of the flow or the geometrical dimensions of the flow facility (pipe diameter,

* Corresponding author.
E-mail address: Matthias.Buschmann@ilkdresden.de (M.H. Buschmann).

0142-727X/$ - see front matter © 2009 Elsevier Inc. All rights reserved.
doi:10.1016/j.ijheatfluidflow.2009.06.004

Nomenclature

a_i, b_i, c_i, d_i	coefficients of Taylor series expansions
u, v, w	velocity components
u_e	velocity at the outer edge of TBL or at channel/pipe center
u_τ	wall skin-friction velocity
Re_θ	Reynolds number based on momentum thickness
Re_b	bulk Reynolds number
y^+	normalized wall-coordinate
α	scaling power
δ	boundary layer thickness
δ^+	Kármán number
κ	Kármán constant of classical logarithmic law

Subscript

∞	infinity
u, v, w, uv	with respect to a certain stress component
p	peak

Superscript

+	classical scaling
$*$	outer scaling
sc	scaling
#	standard mixed scaling
+#	alternative mixed scaling

channel width, etc.). The arduousness following for DNS-calculations is the so-called *supergrid problem* resulting in too small calculation domains that do not cover all relevant energy-containing scales. Taking together it turns out that the derivation of a consistent picture of wall turbulences is overshadowed by several technical problems.

To further complicate the situation, it seems that confined (pipes, channels) and semi-confined flows (boundary layers, wall jets) behave differently even very close to the wall. Here we are interested basically in the separation of physical mechanisms having well distinguished orders of magnitude. In our case, these are the actions of outer scales (top-down effects) and the actions of inner scales (bottom-up effects). Due to the different nature of the flow at the centerline of a channel or pipe flow (only turbulent) and that at the outer edge of a turbulent boundary layer (turbulent and intermittent), these effects are different for confined and semi-confined flow. Additionally there must be a serious difference of $\langle v^2 \rangle$ between cannel and zero-pressure-gradient turbulent boundary layers because the v-fluctuation is strongly connected with pressure.[1] Accepting the influence of outer structures on the near-wall behavior of wall-bounded flows gives automatically arguments for the difference between channel and pipe flows. The w-fluctuation in a channel is not directly affected by the wall at any wall-normal position. This is different for pipe flow where at the centerline the difference between wall-normal and cross-flow fluctuation disappears and the influence of the pipe-wall should be the same on v- and w-fluctuations. This changes when approaching the pipewall.

In this paper, we address the question whether there are ranges in the Reynolds stresses close to the wall that show universal behavior in the sense that they scale with one single length and one single velocity scale. For that purpose, classical inner scaling, standard mixed scaling proposed by DeGraaff and Eaton (2000) and pure outer scaling are studied. Two clearly distinguished features of the stresses, the sublayer behavior and the peak values and positions, are investigated. Similar analysis were undertaken by Sreenivasan (1989), Antonia and Kim (1994), Fernholz and Finley (1996), and others. However, either only a very small number of data was included or several uncertainties following from experiments handicapped their results. To overcome such difficulties, a large DNS-data base for channel flows (CH), pipe flow (PF) and zero-pressure-gradient turbulent boundary layers (ZPG TBL) is compiled. This data base is complemented by several high-quality TBL-experiments.

[1] The authors are grateful to Prof. Yoshijuki Tsuji from Nagoya University for pointing this out to us.

2. Data base

As pointed out by many experimenters, the measurement of Reynolds stress close to the wall is complicated and is susceptible to significant experimental errors, which makes it difficult to investigate scaling effects using physical experiments. Therefore, we compile here a large DNS data base covering Kármán number ranges for pipe and channel flows between 64 and 2006 and for ZPG TBLs between 150 and 1016, as shown in Table 1. Special care was taken when selecting data for very low Kármán numbers to exclude any results that might be affected by insufficiently small calculation domain. This ensures that all relevant scales for the turbulence shear stress are captured. Note that the lowest Kármán number considered here is 64 (Reynolds number based on bulk velocity $Re_b \approx 1844$), which is very close to relaminarization. Reliable conclusions for fully-developed turbulent channel flow might therefore only be drawn down to $\delta^+ = 200$ ($Re_b \approx 6000$). Therefore we will focus on the Kármán number range above 200.

The DNS-data are supplemented by some carfully selected experimental data sets for TBL. The advantage of these data is that they have much higher Reynolds numbers. Their disadvantage is that in some cases they tend to cluster rather by facility than by any physical effect. Some of the high-quality experimental data (McKeon et al., 2004; Zanoun, 2003) offer only mean-velocity profiles. From these data the Reynolds shear stress is predicted employing the mean-momentum equation. With the exception of the ASL data by Priyadarshana and Klewicki (2004), all experimental data are taken over smooth surface. Table 1 gives a comprehensive overview of all data investigated in the present study.

3. Organization of results

The results of the study are compiled in sets of diagrams for each stress. All data use the same color code given in Table 1 for the symbols. Additionally, the diagrams show certain approximation functions. The fully drawn parts of these curves indicate the region where they were calculated from the data (region of validity). Dashed parts indicate extrapolated regions. Special types of dependencies on the Kármán number (constancy, linear or power law behavior) are documented in tables in Section 5. It is our believe that some of the parameters investigated behave asymptotically, reaching constant values only for $Re \to \infty$. However, due to its diminutiveness this asymptotic behavior may not be detectable for finite Reynolds numbers. Therefore, we call all 'constant' values reached *nearly constant*. Each diagram (with exception of Fig. 1) shows a bold vertical line at $\delta^+ = 200$ indicating the border for fully-developed turbulence, as discussed in the previous section. A so-called 3%-border is used to discuss the validity of the first-order

Table 1
Compiled data. CH: channel flow; PF: pipe flow; TBL: turbulent boundary layer; DNS: direct numerical simulations; EXP: experiment; ASL: atmospheric surface layer over rough surface; CMM: calculated employing the mean-momentum balance.

Authors	Kármán number	Type	Symbol
Abe et al. (2004)	180, 365, 640, 1020	CH DNS	
Hoyas and Jiménez (2006)	186, 547, 934, 2006	CH DNS	
Hu et al. (2006)	90, 130, 180, 362, 716, 1451	CH DNS	
Iwamoto et al. (2002)	110, 150, 298, 395, 642	CH DNS	
Laadhari (2002)	120, 160, 180, 235, 589, 1000, 1006, 1461	CH DNS	
Moser et al. (1999)	178, 392, 587	CH DNS	
Tsukahara et al. (2005)	64, 70, 80, 110, 150	CH DNS	
Khujadze and Oberlack (2007)	289, 306, 769, 815, 860, 966, 1016	TBL DNS	
Spalart (1988)	150, 325, 653	TBL DNS	
Wu and Moin (2008)	181, 1143	PF DNS	
Bruns et al. (1992)	970, 1694, 2411, 5582	TBL EXP	
Charlier and Stanislas (2005)	2536, 3987, 5152, 7023	TBL EXP	
DeGraaff and Eaton (2000)	541, 992, 4336, 10,077	TBL EXP	
Ligrani and Bradshaw (1987)	932	TBL EXP	
McKeon et al. (2004)	$(1.8\times10^3 \leqslant \delta^+ \leqslant 5.3\times10^5)$	PF CMM	
Nagano et al. (1992)	407, 507, 586, 656	TBL EXP	
Nickels et al. (2007)	7300	TBL EXP	
Nockemann et al. (1994)	7242, 7577, 13,414, 15,277, 19,050, 20,407	TBL EXP	
Osaka et al. (1998)	355, 480, 776, 1042, 1488, 1697, 1988	TBL EXP	
Priyadarshana and Klewicki (2004)	388, 966, 1493	TBL EXP	
Priyadarshana and Klewicki (2004)	8.9×10^5, 2×10^6, 1.01×10^6	ASL EXP	
Purtell et al. (1981)	311, 870	TBL EXP	
Tsuji et al. (2007)	$(2.3\times10^3 \leqslant \delta^+ \leqslant 7.2\times10^3)$	TBL EXP	
Ueda and Hinze (1975)	502, 1314	TBL EXP	
Zanoun (2003)	$(1.2\times10^3 \leqslant \delta^+ \leqslant 4.8\times10^3)$	CH CMM	

Taylor series expansion of the stresses. This term is explained in detail at the beginning of Reynolds shear stress section.

The majority of the diagrams employ a semi-logarithmic representation, while few are presented on a log–log scale. The advantage of the former representation is that it readily shows whether the Kármán number dependency observed at low δ^+-values dies out when δ^+ approaches infinity. Additionally, the nonlinear representation allows as a first check if a certain Kármán number dependency behaves logarithmically or follows a power law, or if it eventually approaches either relation as $\delta^+ \to \infty$.

4. Classical and mixed scaling

The classical idea of scaling wall turbulence promises that any turbulent quantity scaled with inner variables (u_τ and ν/u_τ) should collapse in a single curve at least in the vicinity of the wall, independently of Reynolds number. That this idea does not work was shown several times especially for the streamwise normal stress. Actually, it was this finding that inspired DeGraaff and Eaton (2000) to employ the so-called mixed scaling.

Classical scaling is essentially near-wall scaling. Any failure of this scaling must therefore be caused by the interaction of near-wall modes with outer modes (Hoyas and Jiménez, 2005; Jiménez and Hoyas, 2008). That near-wall scaling of Reynolds stresses indeed fails was already shown earlier by Townsend (1956, 1976). The outer modes overreach the whole boundary layer (Schlatter et al., 2009) or channel/pipe flow and have much larger length scales than the inner. Therefore, turbulent quantities of wall-bounded flows depend on physical phenomena characterized by well distiguished orders of magnitude. Thus, the effect of different physical mechanisms acting on the turbulent statistics have to be represented by the similarity analysis (see, e.g., Bertola and Cafaro, 2005). Mixed scaling that allows a scaling based on both the characteristic inner (u_τ and ν/u_τ) and the characteristic outer (u_e and δ) scales offers a remedy to cover these effects. The ratio between inner and outer length scales, the Kármán number $\delta^+ = \delta u_\tau/\nu$, is therefore the proper similarity number on which near-wall behavior, peak value and peak position should depend. This is different from many other approaches where these parameters are presented as depending on Re_θ. This Reynolds number is built with the momentum thickness and the outer velocity, which makes it entirely an outer parameter. Consistently similar arguments were used by Buschmann and Gad-el-Hak (2003, 2007) with respect to the mean-velocity profile and led to a generalized logarithmic law covering higher-order Reynolds number effects.

As any other alternative scaling, mixed scaling is motivated by the anticipation of correlating the data in a Reynolds-number-independent way. DeGraaff and Eaton (2000) found that the peak value of the streamwise stress changes proportional to Re_θ^2, which led them to investigate $\langle u^2\rangle^+ \times (u_\tau/u_e)$ (or equvalently $\langle u^2\rangle/u_\tau u_e$). This step is basically a shift of an explicitly observed Reynolds number dependency into the scaling itself, which implies that both the scaling of the stress and some power of the square root of the friction factor can be expanded to first order in the same function of the Reynolds number. A physical explanation for the success of standard mixed scaling was already given by Alfredsson and Johansson (1984). They discovered that the governing time scale of the near-wall region of a channel flow is a mixture of outer and inner scales, and interpreted this as a sign of the interaction of outer and near-wall flows. The mixed time scale employed by Alfredsson et al. (1988) was

$$t_m = \left[\frac{(\nu/u_\tau)\delta}{u_\tau u_e}\right]^{1/2} \tag{1}$$

which already shows the mixed velocity scale used later by DeGraaff and Eaton (2000). Indeed, standard mixed scaling reaches back into the early seventies when Rao et al. (1971) discovered the improved scaling of burst rates per unit span in a turbulent boundary layer when the standard mixed velocity scale $(u_\tau u_e)^{1/2}$ is employed. However, this particular scale may not be universal, as Morrison et al. (2004) showed when they tried to scale the superpipe data.

Sreenivasan (1989), Fernholz and Finley (1996), among others, showed that peak values and positions of the stresses depend on

the Reynolds number. It seems, therefore, reasonable to apply mixed scaling in a more general form to all stresses

$$\langle uv\rangle^{sc} = \frac{\langle uv\rangle}{u_\tau^{2-\alpha}u_e^{\alpha}}; \quad \langle u^2\rangle^{sc} = \frac{\langle u^2\rangle}{u_\tau^{2-\alpha}u_e^{\alpha}};$$
$$\langle v^2\rangle^{sc} = \frac{\langle v^2\rangle}{u_\tau^{2-\alpha}u_e^{\alpha}}; \quad \langle w^2\rangle^{sc} = \frac{\langle w^2\rangle}{u_\tau^{2-\alpha}u_e^{\alpha}} \tag{2}$$

The superscript *sc* denotes the proposed mixed scaling, and the exponent α can take any value between 0 and 2. Classical inner scaling (superscript +) based on u_τ^2 is obtained for $\alpha = 0$. Pure outer scaling (superscript $*$) follows for $\alpha = 2$. For the streamwise Reynolds stress, $\alpha = 1$ and the standard mixed scaling (superscript #) was anticipated by DeGraaff and Eaton (2000) and later successfully employed by Panton (2007). The streamwise stress scales then with $u_\tau u_e$, which gives the same weight to both inner and outer velocity. Here we introduce a new specification of mixed scaling with $\alpha = 0.5$ and viceversa for u_e. Compared with standard mixed scaling, the influence of outer velocity is weaker. In the following, this type of scaling is called "alternative mixed scaling". In any case, the uncertainty caused by experimental errors in u_τ will increase with decreasing α. For DNS-results, uncertainty and error propagation do not play a role because both u_τ and u_e should have the same diminutive numerical error.

Based on Taylor series expansion at $y = 0$, Monin and Yaglom (1971) derived relations for the near-wall behavior of shear and normal stresses scaled classically. Here we rewrite these series in a more general form for mixed scaling with arbitrary power α

$$-\langle uv\rangle^{sc} = -\frac{\langle uv\rangle}{u_\tau^{2-\alpha}u_e^{\alpha}} = \sum_{i=3}^{n} a_i(\delta^+)y^{+i}\left(\frac{u_\tau}{u_e}\right)^{\alpha};$$
$$\langle u^2\rangle^{sc} = \frac{\langle u^2\rangle}{(u_\tau^{2-\alpha}u_e^{\alpha})} = \sum_{i=2}^{n} b_i(\delta^+)y^{+i}\left(\frac{u_\tau}{u_e}\right)^{\alpha};$$
$$\langle v^2\rangle^{sc} = \frac{\langle v^2\rangle}{(u_\tau^{2-\alpha}u_e^{\alpha})} = \sum_{i=4}^{n} c_i(\delta^+)y^{+i}\left(\frac{u_\tau}{u_e}\right)^{\alpha};$$
$$\langle w^2\rangle^{sc} = \frac{\langle w^2\rangle}{(u_\tau^{2-\alpha}u_e^{\alpha})} = \sum_{i=2}^{n} c_i(\delta^+)y^{+i}\left(\frac{u_\tau}{u_e}\right)^{\alpha} \tag{3}$$

That the parameters occurring in (3) are not necessarily universal was already stated by Gad-el-Hak and Bandyopadhyay (1994). A Reynolds number dependency was confirmed by Antonia and Kim (1994), who investigated DNS channel flow data. Bradshaw and Huang (1995), employing the no-slip condition, the no-permeability condition, the continuity equation and the fluctuating part of the momentum equation at $y = 0$, give the first parameters of (3) written for classical scaling as

$$\langle uv\rangle^{+} = \frac{1}{2}\left\langle\frac{\partial u^+}{\partial y^+}\frac{\partial p'^+}{\partial y^+}\right\rangle y^{+3} + \cdots;$$
$$\langle u^2\rangle^{+} = \left\langle\left(\frac{\partial u^+}{\partial y^+}\right)^2\right\rangle y^{+2} + \left\langle\frac{\partial u^+}{\partial y^+}\frac{\partial p'^+}{\partial y^+}\right\rangle y^{+3} + \cdots;$$
$$\langle v^2\rangle^{+} = \frac{1}{4}\left\langle\left(\frac{\partial p'^+}{\partial y^+}\right)^2\right\rangle y^{+4} + \frac{1}{6}\left\langle\frac{\partial p'^+}{\partial y^+}\frac{\partial^2 p'^+}{\partial y^{+2}}\right\rangle y^{+5} + \cdots;$$
$$\langle w^2\rangle^{+} = \left\langle\left(\frac{\partial w^+}{\partial y^+}\right)^2\right\rangle y^{+2} + \left\langle\frac{\partial w^+}{\partial y^+}\frac{\partial p'^+}{\partial y^+}\right\rangle y^{+3} + \cdots \tag{4}$$

Looking at the coefficients of the first-order terms of (4) tells us that longitudinal and cross-flow stress are both different from wall-normal stress in the sense that the last depends, to first order only, on the wall-normal derivative of pressure fluctuation. In his textbook, Davidson (2004) writes *that an eddy (vortex blob) in the core of the flow induces a velocity* [sic pressure] *field which pervades all of the fluid, including the near-wall region.* Due to the differences of the outer regions of ZPG TBL and CH-flows, one may therefore argue that the non-local pressure-related influence of the outer eddies on the turbulence closest to the wall should be geometry dependent. According to (4) this should be visible to first order in the v^2-stress and to second order in the u^2- and w^2-stress. Therefore, the difference between ZPG TBL and CH-flow should be most noticeable in the distributions of the wall-normal Reynolds stress. To obtain the first parameters of each expansion in (3), we write

$$\frac{-\langle uv\rangle^{sc}}{y^{+3}} = a_3^{sc}(\delta^+); \quad \frac{\sqrt{\langle u^2\rangle^{sc}}}{y^{+}} = b_1^{sc}(\delta^+);$$
$$\frac{\sqrt{\langle v^2\rangle^{sc}}}{y^{+2}} = c_2^{sc}(\delta^+); \quad \frac{\sqrt{\langle w^2\rangle^{sc}}}{y^{+}} = d_1^{sc}(\delta^+) \tag{5}$$

All scalings proposed above are strictly based on Buckingham's Π-theorem from 1914 (see, for example, Gersten and Herwig, 1992). This theorem states that any physical process depending on n dimensionally assigned parameters a_j having m independent dimensions could be represented by a relation of $n-m$ non-dimensional similarity numbers Π_i:

$$F(\Pi_1, \Pi_2, \ldots, \Pi_{n-m}) = 0 \tag{6}$$

In general, all similarity numbers have the form of products of powers of the parameters (process variables) a_i:

$$\Pi_i = \prod_{i=1}^{n} a_j^{\gamma_j} \tag{7}$$

where the power γ_j can be any number between $-\infty$ and $+\infty$, as long as the following constraint is satisfied

$$1 = \prod_{i=1}^{n} [a_j]^{\gamma_j} \tag{8}$$

Thus, the normalization $u_\tau^{2-\alpha}u_e^{\alpha}$ proposed with (2) cannot be interpreted as the geometrical mean of two relevant velocity scales. It is merely a product of powers of these two scales. Even more, Buckingham's Π-theorem in general forbids any scaling such as arithmetic or harmonic mean, or any other combination of scales defined as process variables that has a nonmultiplicative structure.[2] However, there is a down side to the Buckingham's Π-theorem, which Bradshaw and Huang (1995) call with respect to the mixing length theory an 'interesting philosophical point', namely *if a theory is dimensionally correct and leads to a result which could be obtained by dimensional analysis alone, the theory need not be physically correct.* This is especially important with respect to the use of u_e in (2) and the following equations. While Morrison (2009) in general rejects u_e as a scaling option, several other approaches employ this parameter successfully (e.g., Panton, 2007). Herein, we will follow the current view of the majority of researchers.

4.1. Reynolds shear stress $\langle \mathbf{uv}\rangle$

Gersten and Herwig (1992) compiled several experimental data of a_3^+ ranging from 4×10^{-4} to 7×10^{-4} and reported an averaged value of 4.1×10^{-4}. A similar value (4×10^{-4}) was given by Sreen-

[2] Note that this does not mean that process variables can not be defined as differences, for example $u_e - u_b$, which eventually appear as factors in similarity numbers.

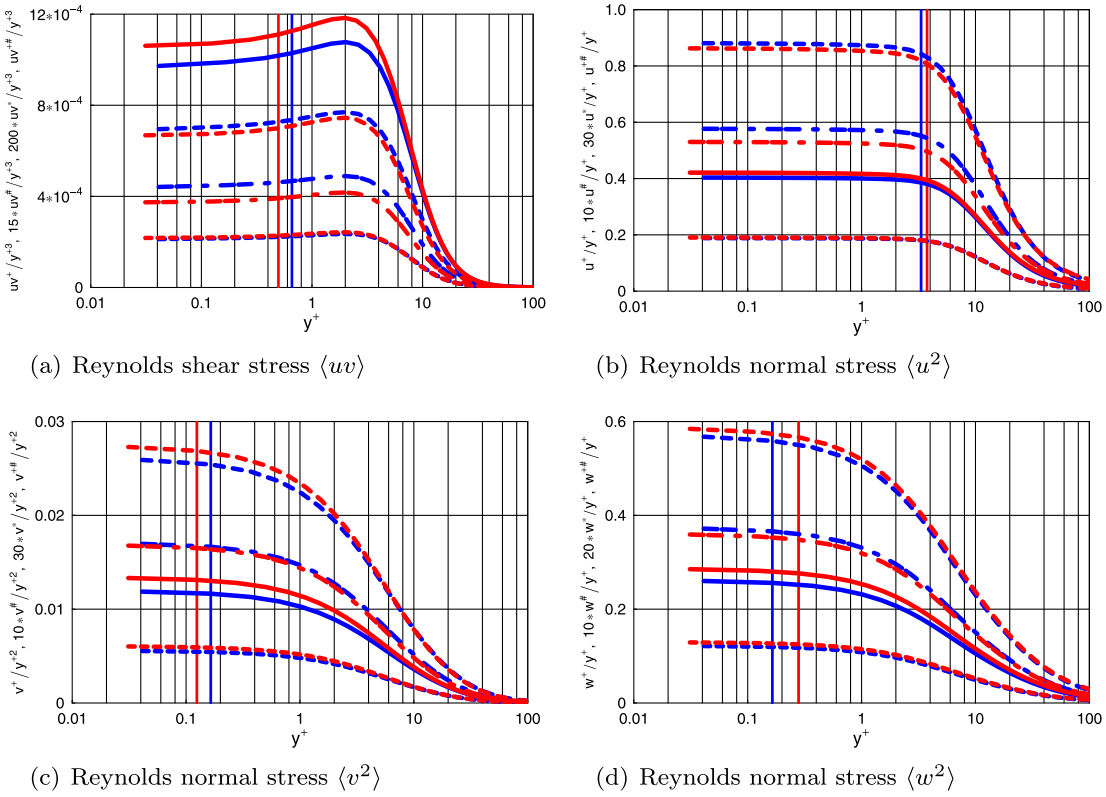

(a) Reynolds shear stress $\langle uv \rangle$ (b) Reynolds normal stress $\langle u^2 \rangle$

(c) Reynolds normal stress $\langle v^2 \rangle$ (d) Reynolds normal stress $\langle w^2 \rangle$

Fig. 1. Comparison of scaling types investigated in the vicinity of the wall. Blue: $\delta^+ = 547$ (Hoyas and Jiménez, 2005); red: $\delta^+ = 1451$ (Hu et al., 2006). Full curves: classical scaling; dashed curves: standard mixed scaling; broken curves: outer scaling; dotted curves: alternative mixed scaling. Vertical lines indicate 3%-border. (For interpretation of the references to colour in this figure legend, the reader is referred to the web version of this article.)

ivasan (1989). The a_3^+ values found here from CH DNS-data are plotted in Fig. 2a and confirm the previous findings for $\delta^+ \lesssim 200$ but exceed them for higher Kármán numbers. The reasons for this discrepancy are manifold. First, we inspect the truncated first-order Taylor series expansion in Fig. 1. For that purpose a region where this approximation gives an acceptable accuracy is defined from the wall to the so-called 3%-border. Up to this y^+ position the percentage change between two consecutive $\langle uv \rangle^{sc}$ values is less than 3%. Note that DNS-data are used for this exercise where the data points are located tightly together ($0.1 \lesssim \Delta y^+ \lesssim 0.6$) in the near-wall region. The 3%-border is therefore quite a sensitive parameter. Below this border the straight horizontal lines in Fig. 1 indicate that the DNS-values are nearly perfectly represented by the truncated Taylor series expansion (5).

For the Reynolds shear stress, the 3% border is found around $y^+ \approx 0.5$—0.7 (see Fig. 1a). The experiments mentioned by Gersten and Herwig (1992) may not have had been so close to the wall to give proper a_3^+-values. This is also the reason why the TBL-data compiled in Table 1 cannot be employed for determining a_3^+. In Fig. 2a the TBL DNS-data by Spalart (1988) and Khujadze and Oberlack (2007) do not fall (with exception of the Khujadze-data with the lowest δ^+) onto the curve of the CH-data. However, neither the CH nor the TBL-data reach a a_3^+ value that is Kármán-number-independent. For the CH-data the situation changes significantly when standard mixed scaling is employed (Fig. 2b). The $a_3^\#$ values are already constant sligthly above $\delta^+ \approx 200$. The TBL-data may cluster around another constant value (see Table 3). Unfortunately the number of TBL DNS realizations is still too low to draw a clear conclusion. The high Reynolds number pipeflow DNS by Wu and Moin (2008) seems to cluster with the high-Reynolds-number TBL DNS by Khujadze and Oberlack (2007) and not with the majority of the channel flow data. Pure outer scaling, depicted in Fig. 2c, fails below $\delta^+ \approx 1000$, but may reach a constant value above this threshold.

Classical theory demands a constant shear stress region for $Re \to \infty$. The ratio $\langle uv \rangle / u_\tau^2$ should then become unity, at least in the vicinity of the peak. However, the DNS-data investigated here show that even for the case with the highest Kármán number, $\delta^+ = 2006$, $\langle uv \rangle_p^+$ reaches only a value of 0.9317 (Figs. 2d and 3a). This falls well into the range of 0.92–0.95 found by Fernholz and Finley (1996) for a Reynolds number range of $2500 \leqslant Re_\theta \leqslant 60,000$ ($1000 \lesssim \delta^+ \lesssim 17,000$). Here we find that below $\delta^+ \approx 1000$ the Kármán number dependence is quite strong. Based on Barenblatt's (1993) power law, a second-order relation for $\langle uv \rangle_p^+$ was derived by Sreenivasan et al. (1997):

$$\langle uv \rangle_p^+ = 1 - \left\{ \frac{(3.1 \pm 0.1)}{\delta^{+(1/2)}} + \frac{0.93}{\delta^{+(1/2)}} \frac{\ln[\ln(\delta^+)]}{\ln(\delta^+)} \right\} \tag{9}$$

Buschmann and Gad-el-Hak (2009a) developed a third-order approximation based on their generalized logarithmic law, which also covers the very low δ^+-range,

$$\langle uv \rangle_p^+ = 1 - \left\{ 1.52 \frac{1}{\delta^{+1/2}} \left[K_G^{\frac{1}{2}} + K_G^{-\frac{1}{2}} \right] + 5.14 \frac{1}{\delta^+} + 32.75 \frac{1}{\delta^{+3/2}} \left[K_G^{\frac{1}{2}} + K_G^{-\frac{1}{2}} \right] \right\} \tag{10}$$

with $K_G = 1 + 64.8/\delta^+$. The functional structure of Eq. (10) and its parameters do not follow from an emprical fit of $\langle uv \rangle_p^+$-data but rather from a higher-order approach for the mean-velocity profile (for details see cited reference). Both relations are in perfect agreement with the high-Reynolds-number pipeflow data by McKeon et al. (2004), the pipeflow DNS by Wu and Moin (2008) and the channel flow data by Zanoun (2003), as shown in Fig. 3a. The

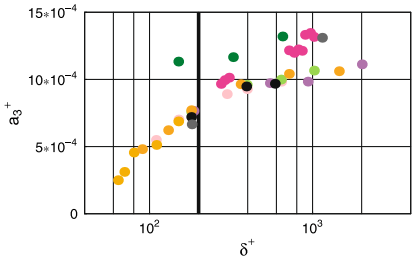

(a) Wall behavior, classical scaling $\alpha = 0$

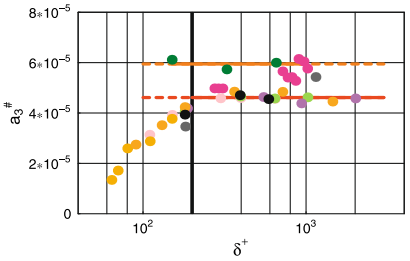

(b) Wall behavior, standard mixed scaling $\alpha = 1.0$. Red line: nearly constant value of DNS CH data above $\delta^+ = 200$; orange line fit of TBL DNS by Spalart (1988)

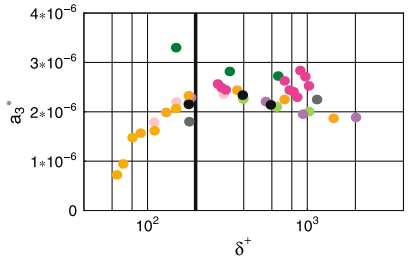

(c) Wall behavior, outer scaling $\alpha = 2.0$

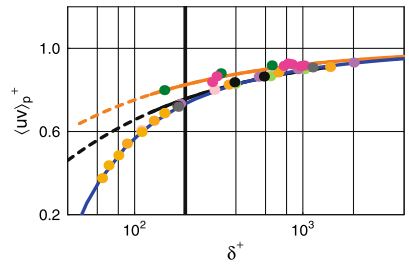

(d) Peak value, classical scaling $\alpha = 0$. Black: Sreenivasan & Sahay (1997); blue: Buschmann & Gad-el-Hak (2008); orange: fit of TBL DNS

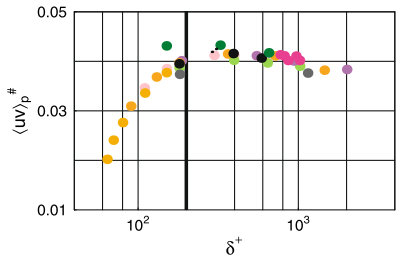

(e) Peak value, standard mixed scaling $\alpha = 1.0$

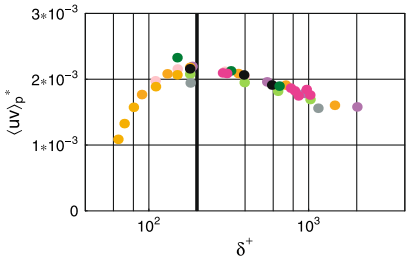

(f) Peak value, outer scaling $\alpha = 2.0$

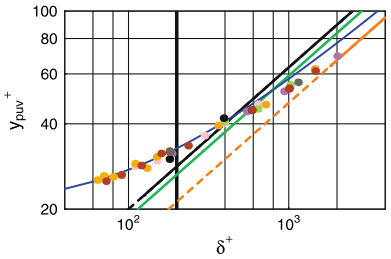

(g) Peak position DNS CH data only. Green: Long & Chen (1981); Black: Sreenivasan & Sahay (1997); orange: Morrison et al. (2004); blue: Buschmann & Gad-el-Hak (2008)

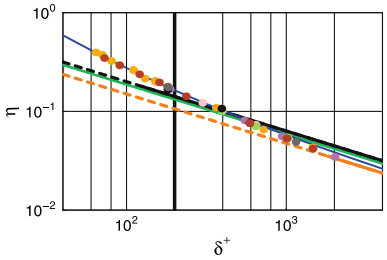

(h) Peak position, outer scaling. Curves as Fig. 2g

Fig. 2. Reynolds shear stress $\langle uv \rangle$.

Table 2
Relations for $\langle u^2 \rangle_p^+$.

Authors	Relation
Klewicki et al. (1994)	$\langle u^2 \rangle_p^+ = 8.5 \times 10^{-9} Re_\theta^2 + 4.8 \times 10^{-4} Re_\theta + 6.86$
Mochizuki and Nieuwstadt (1996)	$\langle u \rangle_p^+ = 1.5 \times 10^{-5} Re_\theta + 2.67$
	Valid for TBL with $200 \leqslant Re_\theta \leqslant 20,920$
	$\langle u \rangle_p^+ = -2.4 \times 10^{-6} \delta^+ + 2.70$
	Valid for internal flow with $100 \leqslant \delta^+ \leqslant 4,300$
Fernholz and Finley (1996)	$\langle u \rangle_p^+ = 0.28 \lg Re_\theta + 1.86$
Metzger (2006)	$\langle u \rangle_p^+ = (0.22 - 0.29) \lg Re_\theta + (1.84 - 2.02)$
Hutchins and Marusic (2007)	$\langle u^2 \rangle_p^+ = 0.965 \ln \delta^+ + 1.036$
	Represents TBL-data above $\delta^+ \leqslant 200$
Present work, Fig. 4d	$\langle u^2 \rangle_p^+ = 0.090 (\ln \delta^+)^2 - 0.571 \ln \delta^+ + 7.627$
	Valid for internal flow with $\delta^+ \gtrsim 100$

low-Reynolds-number TBL-data seem to follow a slightly different trend which can be described with

$$\langle uv \rangle_p^+ = 1 - \frac{2.48}{\delta^{+(1/2)}} \tag{11}$$

The standard mixed scaling shown in Fig. 2e and the outer scaling shown in Fig. 2f do not work, which is in agreement with the classical arguments.

Fig. 2g shows the peak position of the Reynolds shear stress in double logarithmic plot for channel flow. Invoking the local-equilibriums hypothesis and employing the standard log law, a simple approximation function can be derived for internal flows from the mean-momentum equation

$$y_{puv}^+ = \lambda * \delta^{+(1/2)}, \quad \lambda = 1/\kappa^{1/2} \tag{12}$$

Several authors have published values for λ ranging from 1.87 (Long and Chen, 1981) to 2.0 (Sreenivasan et al., 1997) to 1.5 (Morrison et al., 2004). The equivalent κ values would be, respectively, 0.286, 0.250 and 0.444. With the exception of the last one, these values are far from the traditional κ value of 0.41, which may

Table 3
Wall behavior according to different scaling types. All constants and functions are given for $\delta^+ \gtrsim 200$ (Mon. stands for monotonic).

Scaling	$\langle uv \rangle$	$\langle u^2 \rangle$	$\langle v^2 \rangle$	$\langle w^2 \rangle$
Classical inner	Mon. increase $a_3^+(\delta^+)$	$b_1^+(\delta^+) = 0.270 + 0.020 * \delta^+$	Mon. increase $c_2^+(\delta^+)$	Mon. increase $d_1^+(\delta^+)$
Alternative mixed	Mon. increase $a_3^{+\#}(\delta^+)$	$b_{1\infty}^{+\#} = 0.186$	Mon. increase $c_2^{+\#}(\delta^+)$	Mon. increase $d_1^{+\#}(\delta^+)$
Standard mixed	$a_{3\infty}^{\#} = 4.61 \times 10^{-5}$	$b_{1\infty}^{\#} = 8.49 \times 10^{-2}$	Mon. increase $c_2^{\#}(\delta^+)$	Mon. increase $d_1^{\#}(\delta^+)$
Outer	$a_3^*(\delta^+)$	$b_1^*(\delta^+) = 0.027 - 1.31 \times 10^{-3} * \delta^+$	CH: $\delta^+ \gtrsim 200$ $c_{2\infty}^* = 5.55 \times 10^{-4}$ TBL: $\delta^+ \gtrsim 150$ $c_{2\infty}^* = 5.95 \times 10^{-5}$	$d_{1\infty}^* = 1.21 \times 10^{-2}$

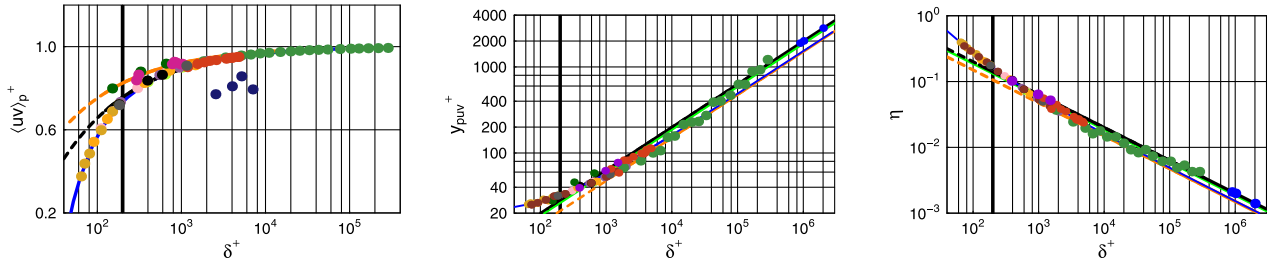

(a) Peak value classical scaling $\alpha = 0$ curves same as Fig. 2d (b) Peak position curves same as Fig. 2g (c) Peak position outer scaling curves same as Fig. 2g

Fig. 3. Peak value and position of Reynolds shear stress $\langle uv \rangle$ including pipe flow data by McKeon et al. (2004), channel flow data by Zanoun (2003) and ASL and TBL-data from Priyadarshana and Klewicki (2004).

indicate low-Kármán-number effects or merely that y_{puv}^+ does not fall into the classical logarithmic region (Antonia et al., 1992). Of course (12) should hold only approximately for flows having sufficiently high Reynolds numbers. Here we find that this is the case above $\delta^+ \approx 600$—1000, as shown in Fig. 2g and Fig. 3b. For lower Kármán numbers, higher-order effects become strong and must be considered. Consistent with Eq. (10), Buschmann and Gad-el-Hak (2009a) give the following second-order approximation for channel flow

$$y_{pG}^+ = 1.521\delta^{+1/2}\left(1 + \frac{64.8}{\delta^+}\right)^{1/2} + 8 \tag{13}$$

which is in reasonable agreement with the data down to the lowest Kármán number (Fig. 2g). Fig. 3b shows an agreement with the superpipe data by McKeon et al. (2004) at least up to $\delta^+ \approx 40,000$. Note that the latter data were calculated from the mean-momentum equation. Neglecting the offset in (13) leads to first order to an equivalent κ-value of 0.432.

The low-Kármán-number effects are also visible in outer scaling of the peak position of the Reynolds shear stress, Fig. 2h. Fig. 3c shows again the outer scaling but includes the pipeflow data by McKeon et al. (2004), the channel flow data by Zanoun (2003), and the atmospheric surface layer data by Priyadarshana and Klewicki (2004). The last confirms the trends depicted in Fig. 2g and h for peak position and value found from low- and medium-Reynolds-number data. However, one has to keep in mind that these data have two significant differences to other data. First, they are taken over rough surface, and, second, an ASL is a wall-bounded flow developing in time and space while a TBL develops in space alone and CH-flows are self-similar. Whether or not the slightly concave behavior of the superpipe data is significant is unclear. At a minimum, it seems to be noteworthy that y_{pu}^+ of TBL does not show such a behavior, as depicted in Fig. 4i.

4.2. Longitudinal Reynolds stress $\langle \mathbf{u^2} \rangle$

The most intensive experimental investigations with respect to the stresses have been conducted for the streamwise fluctuations. Reason is probably that this stress can be measured more accurately than any other using a single hot-wire or a two-beam LDA. Fig. 4a–c show the coefficients $b_1^+(\delta^+), b_1^{\#}(\delta^+)$ and $b_1^*(\delta^+)$ (Fig. 4a). While the experimental values for $b_1^+(\delta^+)$ reported in the literature are mostly constant (0.30, Monin and Yaglom, 1971; 0.36, Kim et al., 1987; 0.39–0.40, Karlsson and Johansson, 1986; Alfredsson et al., 1988; 0.37, Durst et al., 1995; 0.4, DeGraaff and Eaton, 2000), the data analyzed here are clearly Kármán-number-dependent. Wheras the TBL DNS-results show slightly higher values than the CH DNS-data, the experimental values are all below the approximate curve of the channel data. However, all of them indicate the same increasing non-asymptotic trend above $\delta^+ \approx 200$. By contrast, Fischer (1999) investigated low-Reynolds-number DNS and experimental data and found an asymptotic behavior. His curve for experimental data is in perfect agreement with the very-low-Reynolds-number DNS channel flow results by Tsukahara et al. (2005). The standard mixed scaling delivers a nearly constant value of $b_{1\infty}^{\#}$ above $\delta^+ \approx 200$. However, the TBL DNS-data by Kuhjadze (2005) and several experimental data scatter around this value. The 'alternative mixed' scaling (Fig. 4b, $\alpha = 0.5$) is tested here successfully for the first time. The scatter of TBL-data found employing standard mixed scaling is completely removed as shown in Fig. 5a. The pipflow DNS by Wu and Moin (2008) fits very good into the majority of data. In contrast, outer scaling (Fig. 4c) shows a clear Kármán number dependency througout the entire δ^+ range investigated.

Differently from all other stresses, the first-order Taylor series expansion shown in Fig. 1b gives a good approximation much farther away from the wall. The 3% border of the longitudinal shear stress is found around $y^+ \approx 3$—4.

From many experiments it is known, that the $\langle u^2 \rangle^+$ profile of ZPG TBL and CH-flow shows a distinguished peak around $y^+ \approx 15$. However, despite the large number of investigations, the Reynolds number dependency of this parameter remain controversial. Analyzing 47 different experimental works ($Re_\theta = 300 - 20,920; \delta^+ \approx 147$—$7050$), Mochizuki and Nieuwstadt (1996) found nearly constant peak value of 7.34 for zero-pressure-gradient TBL and 7.29 for internal flows. Several other researchers discovered stronger Reynolds number dependencies (Table 2). None of these relations indicate an asymptotic behavior.

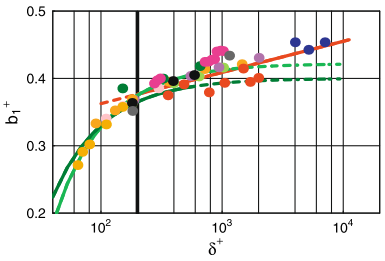

(a) Wall behavior classical scaling $\alpha = 0$ red curve power law fit above $\delta^+ = 200$ green fit exp. data, dark green fit DNS data Fischer (1999)

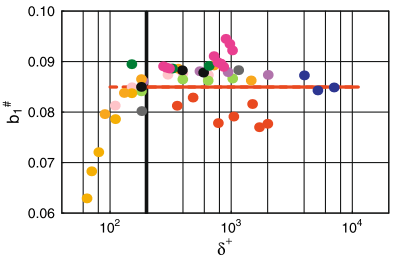

(b) Wall behavior standard mixed scaling $\alpha = 1.0$ red line nearly constant value of DNS CH data above $\delta^+ = 200$

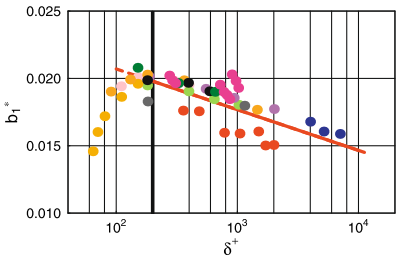

(c) Wall behavior outer scaling $\alpha = 2.0$ red curve power law fit above $\delta^+ = 200$

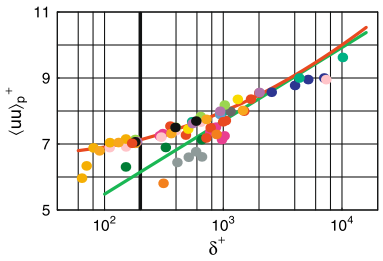

(d) Peak value classical scaling $\alpha = 0$ green curve Hutchins & Marusic (2007), red curve parabolic fit above $\delta^+ = 100$

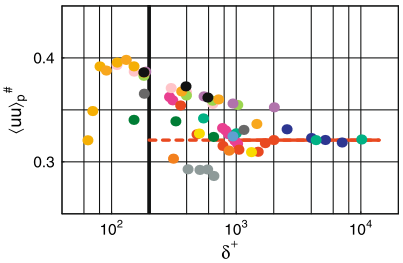

(e) Peak value standard mixed scaling $\alpha = 1.0$ red line nearly constant value for experimental TBL data above $\delta^+ = 1000$

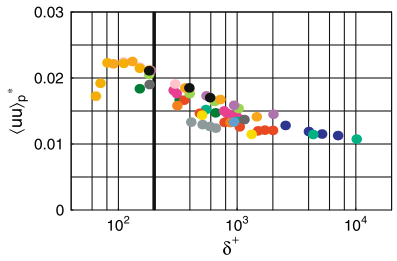

(f) Peak value outer scaling $\alpha = 2.0$

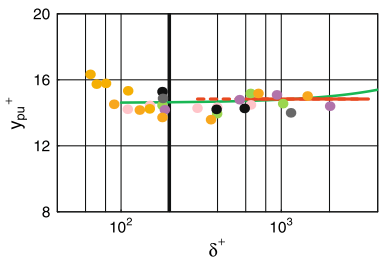

(g) Peak position DNS CH data alone red line nearly constant value above $\delta^+ = 600$, green curve Mochizuki & Nieuwstadt (1996)

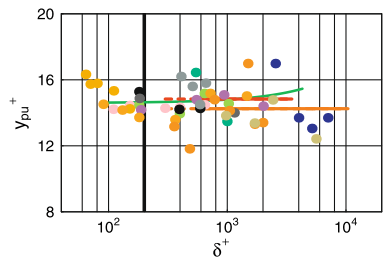

(h) Peak position red and green curve same as Fig. 4g, orange line averaged value of experimental TBL data above $\delta^+ = 600$

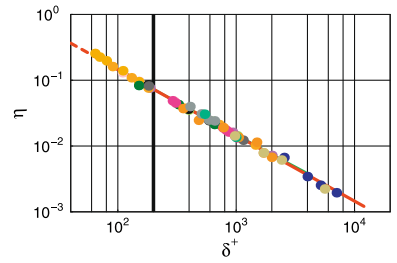

(i) Peak position outer scaling red line power law fit over all data see Table (5)

Fig. 4. Reynolds normal stress component $\langle u^2 \rangle$.

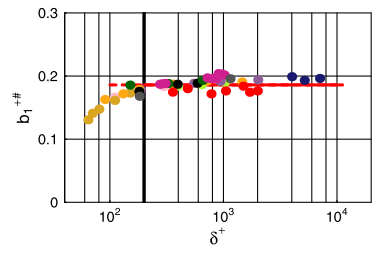

(a) Wall behavior red line nearly constant value above $\delta^+ = 200$

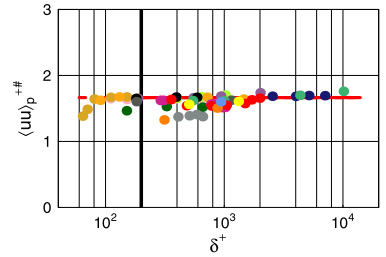

(b) Peak value red line nearly constant value of DNS CH data above $\delta^+ = 100$

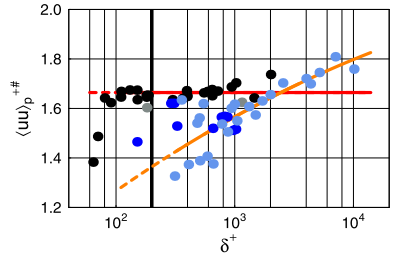

(c) Peak value black symbols CH data, cornflowerblue experimental and blue DNS TBL data, gray pipe DNS, red curve as Fig. 5a, orange fit experimental TBL data above $\delta^+ = 300$

Fig. 5. Alternative mixed scaling ($\alpha = 0.5$) for Reynolds normal stress component $\langle u^2 \rangle$.

Even the ASL data by Metzger and Klewicki (2001) confirm that the peak value of the streamwise stress increases indefinitely when scaled with u_τ^2. This finding is consistent with our own analysis (see Fig. 4d) and goes together with the non-asymptotic behavior of b_1^+ discussed in the previous paragraph. The majority of the TBL-data below $\delta^+ \approx 1000$, both DNS and experiment, lies below the CH DNS-data. This supports the idea that TBL and CH peak values behave differently (see, e.g., Hutchins and Marusic, 2007). However, a clear conclusion cannot be drawn from the data investigated herein. Reason is mainly the scarcity of TBL DNS-data.

For standard mixed scaling (Fig. 4e), a nearly constant value of $\langle u^2\rangle^{\#}_{p\infty}$ for ZPG TBL seems to be reached above a Kármán number of about 1000. The CH DNS-data show after a local peak at about $\delta^+ \approx 140$ a monotonic decrease and may reach a slightly higher value of $\langle u^2\rangle^{\#}_{p\infty}$ as TBL above $\delta^+ \approx 2000$. Pure outer scaling (Fig. 4f) seems to fail at least in the δ^+-region investigated here.

Considering a law of the wall-wake formulation for the mean-velocity profile, Marusic and Kunkel (2003) concluded for standard mixed scaling

$$\langle u^2\rangle^{\#}_{p\infty} = \frac{\langle u^2\rangle_{p\infty}}{u_\tau u_e} = c_1\kappa \tag{14}$$

Here c_1 denotes the coefficient of the logarithmic term in their $\langle u^2\rangle^+_p$ relation (Table 2). For $\kappa = 0.38 - 0.41$ and $c_1 = 0.965, \langle u^2\rangle^{\#}_{p\infty} = 0.367 - 0.396$, which is about 10% to 20% larger than the value of 0.321 found here (see also Table 4). Metzger (2006) analysing measurements in ASL and laboratory data gave with 0.325 a much closer value.

The alternative mixed scaling is successfully applied for channel flow and pipeflow in Fig. 5b, which indicates that a constant value of $\langle u^2\rangle^{+\#}_{p\infty}$ is already achieved around $\delta^+ \approx 100$. This is obviously not the case for ZPG TBL as indicated in Fig. 5c. Despite the experimental error that may overshadow the differences between both types of flows, the trend of the TBL-data is clearly different from that of the CH and pipeflow data. This again indicates that direct interaction between large and small scales exist in TBL, which cannot be removed by simple superposition of scales (see, e.g., Metzger and Klewicki, 2001). A nonlinear fit of the experimental data compiled here gives the following approximation curve for Kármán number above 300.

$$\langle u^2\rangle^{+\#}_p = -6.42\times 10^{-3}(\ln\delta^+)^2 + 0.204\ln\delta^+ + 0.463 \tag{15}$$

Fig. 4g–i show the peak position of the streamwise stress. Beyond a weak depression around $\delta^+ \approx 200$—600 (see Fig. 4g), this parameter reaches, a constant value of 14.84 for the DNS CH-data and 14.25 for all the other data compiled. DeGraaff and Eaton (2000) reported a smaller value of 14 for TBL. In their review paper, Mochizuki and Nieuwstadt (1996) found the following Reynolds-number-dependent relations for channel flow

$$y^+_{pu} = 0.00020\delta^+ + 14.6; \quad 100 \leqslant \delta^+ \leqslant 4300 \tag{16}$$

and for boundary layers

$$y^+_{pu} = 0.00017Re_\theta + 14.4; \quad 300 \leqslant Re_\theta \leqslant 20,920 \tag{17}$$

Fig. 4g shows that relation (16) is in fairly good agreement with the CH-data. The mean value of 14.9 for TBL reported by Mochizuki and Nieuwstadt (1996) is slightly higher than the value found here. In outer variables all data order on an exact straight line in double-log plot, as seen in Fig. 4i. Relation (16) is nearly not visible because it is entirely covered by the symbols and our own approximation given in Table 5. Employing outer scaling no significant differences between ZPG TBL and CH-data can be detected.

4.3. Wall-normal Reynolds stress $\langle \mathbf{v^2}\rangle$

The wall-normal fluctuations are of great importance because they provide the effective turbulence transport, one of the main feature of turbulent wall-bounded flows (for a detailed discussion see, e.g., Fernholz and Finley, 1996). Differently from streamwise and cross-flow fluctuations, the wall-normal component is strongly influenced by the impermeability of the wall. Our results for the v fluctuations are compiled in Fig. 1c, Fig. 6 and Fig. 7. In general, the near-wall behavior of $\langle v^2\rangle$ is quite different from the one for the streamwise stress. The peak occurs much farther away from the wall and is much more shallow. Collecting some older data, Gad-el-Hak and Bandyopadhyay (1994) have already concluded that inner (classical) scaling does not work for $\langle v^2\rangle$ across the entire viscous region. A similar observation has been reported by Fernholz and Finley (1996) who stated that "there is little or no sign of similarity". Both results are based on experiments and one should keep in mind the experimental difficulties associated with measuring the v-component. However, theoretical arguments on the difference of the profiles of the two wall-parallel and the one wall-normal fluctuations were already given by Townsend (1956, 1976) by his formulation of the attached eddy model. A detailed recent discussion with that respect can be found in Jiménez and Hoyas (2008).

The truncated first-order Taylor series expansion (Fig. 1c) represents the wall-normal stress only within a minute region very close to the wall. The 3% border is found at y^+ value between 0.1 and 0.2, as shown in Fig. 1c. The determination of the first surviving coefficient of the truncated Taylor series expansion c_2^{sc} is difficult. Unfortunately, none of the experimental data from Table 1 comes close enough to the wall to deliver reliable values for c_2^{sc} and no values are reported in the literature. An exception are the c_2^+ values derived by Antonia and Kim (1994) from CH DNS-data, which show a clear Kármán number dependency (Fig. 6a). Investigating the DNS-data compiled herein confirms this dependency. However, the δ^+ range covered here is too small to find out if c_2^+ reaches an asymptotic state as $\delta^+ \to \infty$. The situation is similar for standard mixed scaling (Fig. 6b), which makes it hopeless to look at the in-between alternative mixed scaling. Surprisingly, however, the outer scaling (6c) with $\langle v^2\rangle^* = \langle v^2\rangle/u_e^2$ is doing quite a good job in the sense that a nearly constant value of $c^*_{2\infty}$ is achieved above $\delta^+ \approx 200$. In any case, the DNS TBL-data mainly do not fall into the curves generated by the CH-data and may cluster around another constant value (see Table 3). Because only DNS-data with similar high-quality are employed, this difference may well indicate the general difference between channel and boundary-layer flows.

The situation is different for the peak value of the wall-normal Reynolds stress. Here the alternative mixed scaling works fine as shown in Fig. 7, while pure outer scaling totally fails in approaching a Kármán-number independent state (Fig. 6f). The alternative mixed scaling (7a) works even better for the TBL-data having the highest Reynolds numbers (Nockemann et al., 1994). Classical scaling (Fig. 6d) shows a clear increase of the peak value above $\delta^+ \approx 1000$ follows:

$$\langle v^2\rangle^+_p = 0.686 + 0.070\log(\delta^+) \tag{18}$$

It should be mentioned that Priyadarshana et al. (2007) also reported a very weak increase of $\langle v^2\rangle^+_p$ for values for Re_θ larger than about 1500 ($\delta^+ \gtrsim 700$). Unlike the streamwise stress component shown previously in Fig. 5c, no differences between confined and semi-confined flows can be detected for the peak value of the wall-normal Reynolds stress, as shown in Fig. 7b.

The peak position y^+_{pv} depends strongly and non-asymptotically on the Kármán number (Fig. 6g and h). This is in agreement with Sreenivasan (1989):

Table 4
Peak value according to different scaling types.

Scaling	$\langle uv\rangle$	$\langle u^2\rangle$	$\langle v^2\rangle$	$\langle w^2\rangle$
Classical inner	Mon. increase $\langle uv\rangle_p^+(\delta^+)$ see Eq. (10)	Mon. increase $\langle u^2\rangle_p^+(\delta^+)$ CH: see Table 2	Mon. increase $\langle v^2\rangle_p^+(\delta^+)$ see Eq. (18)	Mon. increase $\langle w^2\rangle_p^+(\delta^+)$
Alternative mixed	Mon. increase $\langle uv\rangle_p^{+\#}(\delta^+)$	CH: $\delta^+ \gtrsim 100$ $\langle u^2\rangle_{p\infty}^{+\#} = 1.664$ TBL: mon. increase see Eq. (15)	$\delta^+ \gtrsim 1000$ $\langle v^2\rangle_{p\infty}^{+\#} = 0.242$	Mon. increase $\langle w^2\rangle_p^{+\#}(\delta^+)$
Standard mixed	$\langle uv\rangle_p^{\#}(\delta^+)$	TBL: $\delta^+ \gtrsim 1000$ $\langle u^2\rangle_{p\infty}^{\#} = 0.321$	$\langle v^2\rangle_p^{\#}(\delta^+)$	$\delta^+ \gtrsim 1000$ $\langle w^2\rangle_{p\infty}^{\#} = 0.093$
Outer	$\langle uv\rangle_p^{*}(\delta^+)$	$\langle u^2\rangle_p^{*}(\delta^+)$	$\langle v^2\rangle_p^{*}(\delta^+)$	$\langle w^2\rangle_p^{*}(\delta^+)$

Table 5
Peak position according to different scaling types.

Scaling	$\langle uv\rangle$	$\langle u^2\rangle$	$\langle v^2\rangle$	$\langle w^2\rangle$
Classical inner	Mon. increase $y_{puv}^+(\delta^+)$CH see Eq. (13)	$\delta^+ \gtrsim 600$ CH alone $y_{pu\infty}^+ = 14.84$ CH and TBL $y_{pu\infty}^+ = 14.25$	Mon. increase CH see Eq. (21) TBL see Eq. (22)	$\delta^+ \gtrsim 150$ CH see Eq. (24)
Outer	Mon. decrease $\eta_{puv}(\delta^+)$	$\eta_{pu}(\delta^+) = 14.670/\delta^+$	CH: $\delta^+ \gtrsim 200$ $\eta_{pv}(\delta^+) = 11.842/\delta^{+0.7}$ TBL: $\delta^+ \gtrsim 2000$ $\eta_{pv\infty} = 0.227$	$\delta^+ \gtrsim 150$ $\eta_{pw}(\delta^+) = 22.031/\delta^{+0.908}$

$$y_{pv}^+ = \delta^{+0.75} \tag{19}$$

and Fernholz and Finley (1996):

$$y_{pv}^+ = 0.071 \times Re_\theta \tag{20}$$

whos functions are likewise shown[3] beside our fits in Fig. 6h. From the data analyzed here we obtain the following relation for channel flows

$$y_{pv}^+ = 11.842 * \delta^{+0.300} \tag{21}$$

and for turbulent boundary layers

$$y_{pv}^+ = 0.227 * \delta^{+0.973} \tag{22}$$

From his findings, Sreenivasan (1989) concluded "that v-fluctuations are essentially an outer layer and therefore inviscid phenomenon". One of the most impressing results of the present study is the clear difference between the peak position of confined (channel) and semi-confined (boundary layer) flows, as depicted in Fig. 6h and i. Plotted in inner variables, Fig. 6h shows that the peak position of channel flow is much closer to the wall than the peak position of TBL. Plotted in outer variables ($\eta_{pv} = y_{pv}/\delta$), the TBL-data reach a constant value above $\delta^+ \approx 400$. Note that this is confirmed by four independent experimental data sets (Bruns et al., 1992; Nockemann et al., 1994; Carlier and Stanislas, 2005; Tsuji et al., 2007). Such a strong difference is not visible in the y_{pu}^+- and the y_{pw}^+-distributions, respectively Figs. 4 and 8i. A possible explanation is that $\langle v^2\rangle$ is indeed strongly influenced by outer scales, which are different for semi-confined and confined flows. Even stronger, while in the latter the outer flow is only turbulent and the outer length scale can either be imposed by the flow geometry and/or large-scale outer structures, the flow at the boundary layer edge is turbulent and intermittent and the outer length scale can only be imposed by large-scale outer structures. A similar idea was already expressed by Alfredsson and Johansson (1984). More data in the range of $10^3 \leqslant \delta^+ \leqslant 10^4$ are needed to answer this question more definitively.

[3] The relation $\delta^+ = 1.168 \times Re_\theta^{0.875}$ was considered to employ the Fernholz–Finley function.

4.4. Cross-flow Reynolds stress $\langle \mathbf{w^2} \rangle$

Similar to the v-fluctuations, the wall behavior of the cross-flow component can only be investigated employing DNS-data. None of the experimental data from Table 1 reach sufficiently close to the wall to be able to reliably predict d_1^{sc}. An exception is the experiment by Durst et al. (1995) who gave for pipeflow with $\delta^+ = 500$ a d_1^+ value of 0.21. This is well within the range found here in Fig. 8a. In general, the coefficient d_1^+ shows an asymptotic behavior across the entire δ^+ range investigated. Employing standard mixed (Fig. 8b) scaling may lead to a nearly constant value of $d_{1\infty}^{\#}$, for $\delta^+ > 1000$. However, pure outer scaling (Fig. 8c) leads to the best result where a constant d_1^* is already attained from $\delta^+ \approx 200$ upward.

The first-order Taylor series expansion (Fig. 1d) works fine in a region slightly larger than that for the v-fluctuations, but again much smaller as compared to the region for the u-fluctuations. The 3%-border is found around $y^+ \approx 0.2$–0.3, as shown in Fig. 1d.

All peak values of $\langle w^2\rangle_p^+$ order quite well along one curve, which seems not to approach an asymptotical limit, as shown in Fig. 8d. An exception is the high-Reynolds-number data set by Nockemann et al. (1994). However, even these data confirm the finding by Fernholz and Finley (1996) that $\langle w^2\rangle_p^+$ rises from 2 for $Re_\theta = 670$ ($\delta^+ \approx 347$) to about 3 for higher Reynolds numbers. Priyadarshana et al. (2007) published a relation for $\langle w^2\rangle_p^+$ based on low-Reynolds-number laboratory data as well as data from high-Reynolds-number atmospheric surface layer

$$\langle w^2\rangle_p^+ = 0.256 * \log(Re_\theta) + 0.742 \tag{23}$$

By slightly adjusting the additive constant from 0.742 to 0.6, a very good agreement between (23) and the data is achieved above $\delta^+ \approx 400$, as shown in Fig. 8d. Standard mixed scaling (Fig. 8e) works well and delivers a constant value $\langle w^2\rangle_{p\infty}^{\#}$ for $\delta^+ \gtrsim 800$. Alternative mixed scaling seems not to be as effective (see Fig. 9). Obviously the influence of outer-velocity scales on the peak value of the w-fluctuations is stronger than the one on the peak value of the u- and v-fluctuations. As shown in Fig. 8f, outer scalings again fails to approach an asymptotic state. None of the scaling types indicates any significant distinction between CH- and TBL-data (see especially Fig. 9b).

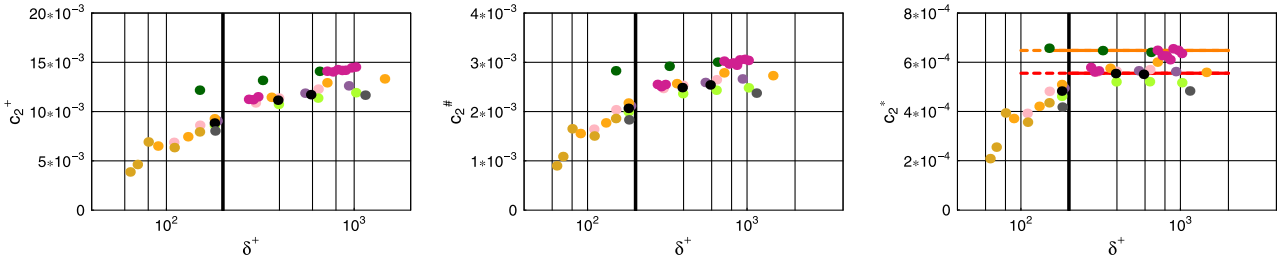

(a) Wall behavior classical scaling $\alpha = 0$ (b) Wall behavior standard mixed scaling $\alpha = 1.0$ (c) Wall behavior outer scaling $\alpha = 2.0$ red line nearly constant value of DNS CH data above $\delta^+ = 200$; orange line fit of TBL DNS by Spalart (1988)

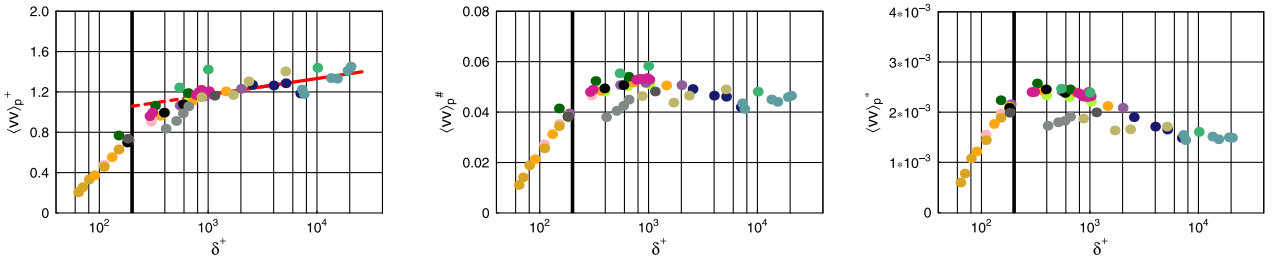

(d) Peak value classical scaling $\alpha = 0$ red line power law fit above $\delta^+ = 1000$ (e) Peak value standard mixed scaling $\alpha = 1.0$ (f) Peak value outer scaling $\alpha = 2.0$

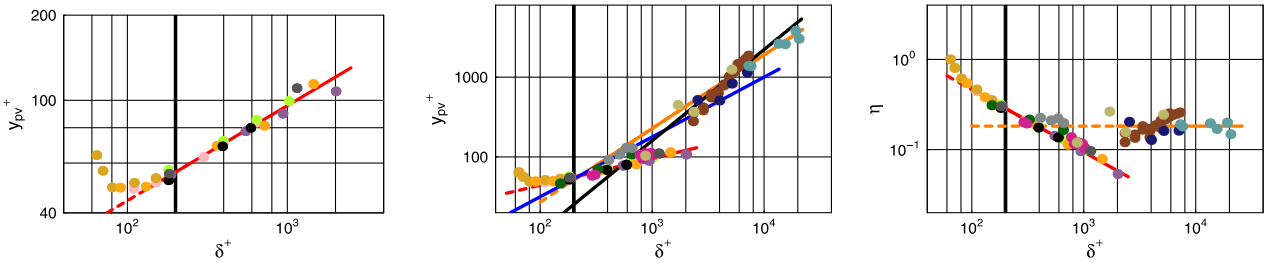

(g) Peak position red line power law fit of DNS CH data above $\delta^+ = 150$ (h) Peak position red line as Fig. (6g), orange line power law fit of experimental TBL data above $\delta^+ = 200$, blue line Sreenivasan (1989), black line Finley & Fernholz (1996) (i) Peak position outer scaling red line power law fit of DNS CH data above $\delta^+ = 200$, orange line nearly constant value of experimental TBL data above $\delta^+ = 2000$

Fig. 6. Reynolds normal stress component $\langle v^2 \rangle$.

Fernholz and Finley (1996) stated in their review that y_{pw}^+ is a function of Re_θ and ranges between 20 and 50. Due to the large scatter of the data, however, the authors avoided plotting them. For the same reason, Sreenivasan (1989) could not find a clear trend. The CH and pipe flow DNS-data analyzed here show such a trend, which is obviously similar as for y_{pv}^+.

$$y_{pw}^+ = 22.031 * \delta^{+0.092} \tag{24}$$

The position of the peak y_{pw}^+ is perspicuously closer to the wall than y_{pv}^+ but still much farther away as compared to y_{up}^+. Still, the experimental TBL-data have a pronounced scatter so that no evidence can be drawn from them (Fig. 8h). The scatter is less visible when plotted in outer variables. Again, a linear decrease is found in the double-log plot shown in Fig. 8i.

None of the representations of cross-flow fluctuation parameters shows any significant differences between semi-confined and confined flow.

5. Conclusions

A data base compiling a large number of results from direct numerical simulations and physical experiments was used to explore the properties of shear and normal Reynolds stresses very close to the wall of channel/pipe flows and boundary layers with zero pressure gradient. Three types of scaling were investigated, classical inner, standard mixed, and pure outer scaling. To qualify the influence of outer scales more precisely, a new scaling called *alternative mixed scaling* based on $u_\tau^{3/2} u_e^{1/2}$ was introduced. All results are compiled in plots and summarized in Tables 3–5.

With respect to the four types of scaling, no conclusion in the sense of *And the winner is* ... can be drawn. That clearly indicates that the different outer and inner scales of wall-bounded flows act differently on the three fluctuations. For almost all parameters investigated, classical inner scaling shows a clear dependence on the Kármán number. The only exception from that finding is the

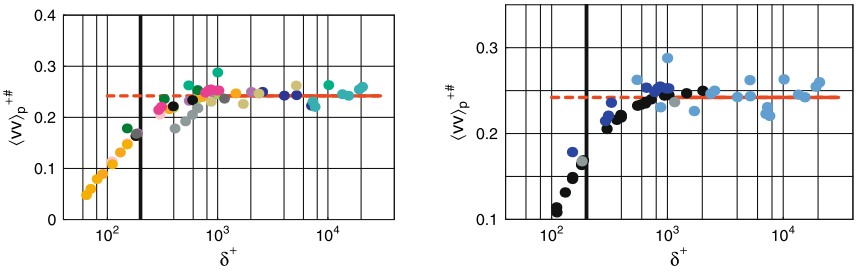

(a) Red line nearly constant value of experimental TBL data above $\delta^+ = 1000$

(b) Black symbols CH data, cornflowerblue experimental (without Nagano et al. 1992) and blue DNS TBL data, gray pipe DNS, red curve as Fig. 7a

Fig. 7. Peak value of Reynolds normal stress component $\langle v^2\rangle$ for alternative mixed scaling $\alpha = 0.5$.

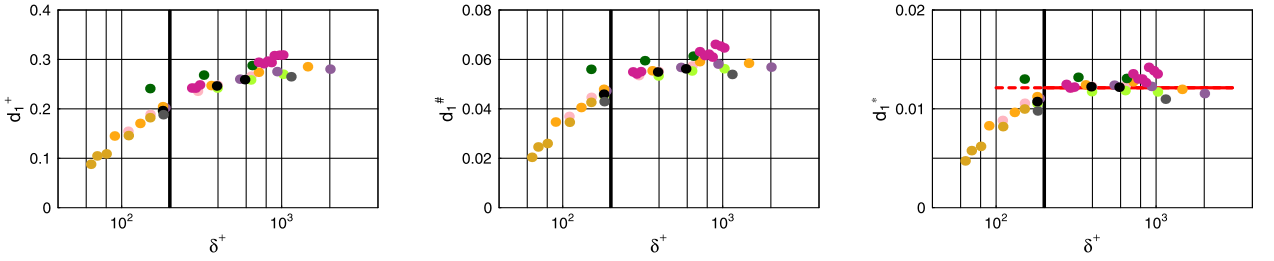

(a) Wall behavior classical scaling $\alpha = 0$

(b) Wall behavior standard mixed scaling $\alpha = 1.0$

(c) Wall behavior outer scaling $\alpha = 2.0$ red line nearly constant value of DNS CH data above $\delta^+ = 200$

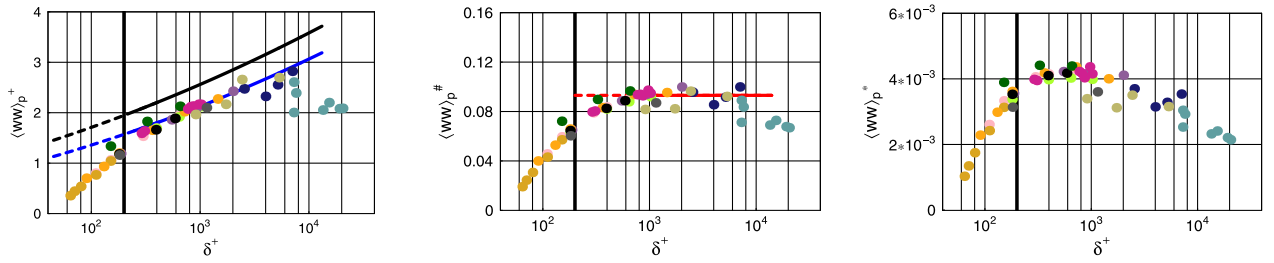

(d) Peak value classical scaling $\alpha = 0$ dark green curve Priyadarshana et al. (2007), red curve modified Eq. (23)

(e) Peak value standard mixed scaling $\alpha = 1.0$ red line nearly constant value of all data above $\delta^+ = 1,000$ without Nockemann et al. (1994)

(f) Peak value outer scaling $\alpha = 2.0$

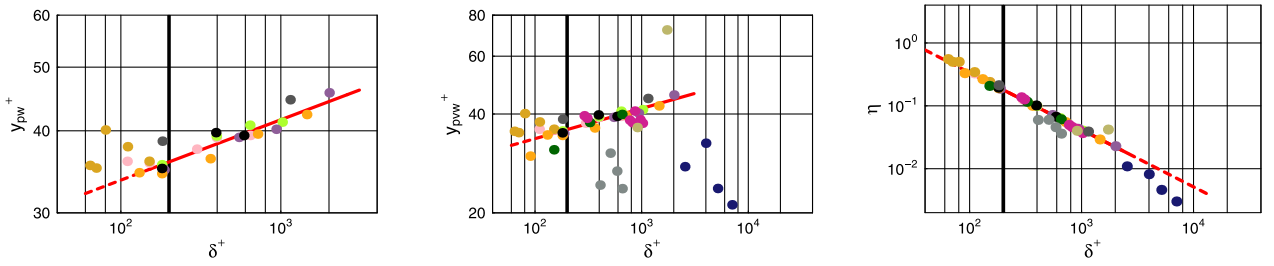

(g) Peak position red line power law fit of DNS CH data above $\delta^+ = 600$

(h) Peak position red line same as Fig. 8g

(i) Peak position outer scaling red line power law fit of DNS CH data above $\delta^+ = 60$

Fig. 8. Reynolds normal stress component $\langle w^2\rangle$.

peak position of $\langle u^2\rangle$. This parameter has a nearly constant value of 14.25–14.84 above $\delta^+ \approx 600$. The Kármán number is the proper independent variable because it deliberates the ratio of inner and outer length scales. In certain cases, alternative mixed scaling is superior to the standard mixed scaling based on $u_\tau u_e$, proposed by DeGraaff and Eaton (2000).

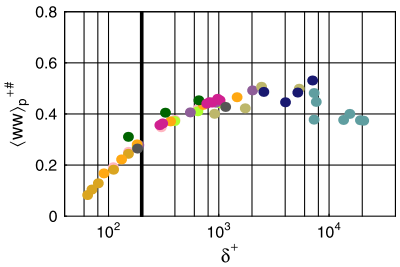

(a) Peak value

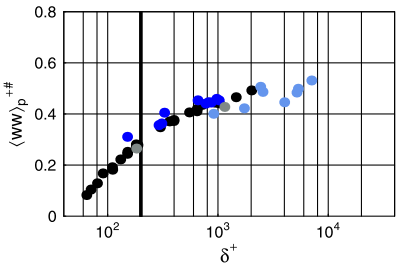

(b) Black symbols CH data, cornflowerblue symbols experimental (without Nagano et al. 1992 and Nockemann et al. 1994) and blue DNS TBL data

Fig. 9. Peak value of Reynolds normal stress component $\langle w^2 \rangle$ for alternative mixed scaling $\alpha = 0.5$.

In a personal communication, J. F. Morrison from Imperial College London pointed out that *in conformity with Newton's second law, accelerations or velocity differences (and not velocities) describe the dynamical behavior because they are frame invariant. However, the use of Reynolds decomposition invites us to consider velocity scales for both the turbulence as well as the mean flow*. The *argumentum e contrario* is that the Reynolds decomposition is in principle not suitable to describe the dynamical behavior of wall-bounded flows. From that point of view, a triple decomposition for instantaneous velocities *and* vorticities, as proposed by Hussain (1986), may be more suitable to capture the dynamics of the flow. In any case, we have to state that complete fluid mechanical similarity is constituted by three components, namely geometrical, kinematical and dynamical. Only if all three are satisfied for two different flows would those flows be considered completely fluid-mechanically similar. For example, this should be the case for the flow at two different streamwise positions of the same channel, but not for two channels with different Reynolds numbers. Therefore, the present study is basically a contest to capture kinematic similarity. To obtain this partial similarity is a necessary but not sufficient condition to identify complete fluid mechanical similarity. A step further may be found in studies that are based on essential features of the turbulent flow such as energy transfer and related Kolmogorov scales (Wagner et al., 2001; Stanislas et al., 2008; Buschmann et al., in press).

The major results of the present study are as follows:

1. The first-order Taylor series expansions going back to Monin and Yaglom (1971) work satisfactorily only in a very limited region extremely close to the wall. Plotting the first-order coefficients of these series employing classical inner scaling, it is found that all of them show more or less an asymptotic dependence on δ^+. However, constant values are not reached below $\delta^+ \approx 2000$. For $\langle uv \rangle$ employing standard mixed scaling, for $\langle u^2 \rangle$ employing alternative mixed scaling, and for $\langle v^2 \rangle$ and $\langle w^2 \rangle$ employing pure outer scaling, strengthening the dependence on the outer-velocity scale leads to Kármán-number-independent coefficients above $\delta^+ \approx 200$.
2. Significant differences between confined and semi-confined flows are found for the peak value of $\langle u^2 \rangle$ for low Kármán number, and the peak position of $\langle v^2 \rangle$ for Kármán numbers larger than 200. However, number and quality of data are still too low to draw firm conclusions with respect to $\langle u^2 \rangle_p$. Due to the influence of pressure gradient on the wall-normal fluctuation the later finding seems plausible. Differences between channel and zero-pressure-gradient turbulent boundary layers were also found for the peak value of Reynolds shear stress up to $\delta^+ \approx 1000$. Weak differences between the wall behaviors were also discovered for Reynolds shear stress and wall-normal stress.
3. Employing classical inner scaling shows that all peak values increase with δ^+. While the $\langle uv \rangle$- and the $\langle v^2 \rangle$-peak distributions may reach an asymptotic state, the $\langle u^2 \rangle$- and $\langle w^2 \rangle$-peaks increase non-asymptotically with Kármán number. While alternative mixed scaling leads to constant peak values for $\langle u^2 \rangle$ and $\langle v^2 \rangle$, standard mixed scaling does the same for $\langle w^2 \rangle$. Pure outer scaling fails in achieving constant peak values for all cases.
4. Scaled with classical inner variables, the peak positions of $\langle uv \rangle, \langle v^2 \rangle$ and $\langle w^2 \rangle$ increase non-asymptotically. In all cases, the dependence on δ^+ follows a power law but with different coefficients. The peak position of $\langle u^2 \rangle$ is nearly constant.
5. Plotting the peak positions employing outer variables it is found, that all distributions follow power laws in δ^+. An exception is the peak position of $\langle v^2 \rangle$, which reach a constant value for zero-pressure turbulent boundary layers above $\delta \approx 2000$.

The study showed clear trends and tendencies. However, more experimental data close to the wall and more DNS-results having higher Reynolds numbers are urgently needed to complete the picture of turbulence closest to the wall.

Acknowledgement

We thank all scientists who supported us with their data.

References

Abe, H., Kawamura, H., Matsuo, Y., 2004. Surface heat-flux fluctuations in a turbulent channel flow up to $Re = 1020$ with $Pr = 0.025$ and 0.71. Int. J. Heat Fluid Flow 25, 404–419.

Adrian, R.J., 2007. Hairpin vortex organization in wall turbulence. Phys. Fluids 19, 041301.

Alfredsson, P.H., Johansson, A.V., 1984. Time scale in turbulent channel flow. Phys. Fluids 31, 1974–1981.

Alfredsson, P.H., Johansson, A.V., Haritonidis, J.H., Eckelmann, H., 1988. The fluctuating wall-shear stress and the velocity field in the viscous sublayer. Phys. Fluids 31, 1026–1033.

Antonia, R.A., Kim, J., 1994. Low-Reynolds-number effects on near-wall turbulence. J. Fluid Mech. 276, 61–80.

Antonia, R.A., Teitel, M., Kim, J., Browne, L.W.B., 1992. Low-Reynolds-number effects in a fully developed turbulent channel flow. J. Fluid Mech. 236, 579–605.

Barenblatt, G.I., 1993. Scaling laws for fully developed turbulent shear flows Part 1. Basic hypotheses and analysis. J. Fluid Mech. 248, 513–520.

Bertola, V., Cafaro, E., 2005. Intermediate asymptotic behaviour of fluid flows by scalesize analysis. Philos. Trans. R. Soc. A 461, 755–760.

Bradshaw, P., Huang, G.P., 1995. The law of the wall in turbulent flow. Proc. R. Soc. Lond. A 451, 165–188.

Bruns, J., Dengel, P., Fernholz, H.H., 1992. Mean flow and turbulence measurements in an incompressible two-dimensional turbulent boundary layer Part I: data. Herman-Fôttinger Institut für Thermo- und Fluiddynamik, TU-Berlin.

Buschmann, M.H., Gad-el-Hak, M., 2009a. Evidence of non-logarithmic behavior of turbulent channel and pipe flow. AIAA J. 47, 535–541.

Buschmann, M.H., Gad-el-Hak, M., in press. Kolmogorov scaling of turbulent flow in the vicinity of the wall. Physica D, doi:10.1016/j.physd.2009.07.006.

Buschmann, M.H., Gad-el-Hak, M., 2007. Recent developments in scaling of wall-bounded flows. Prog. Aerospace Sci. 42, 419–467.

Buschmann, M.H., Gad-el-Hak, M., 2003. Generalized logarithmic law and its consequences. AIAA J. 41, 40–48.

Buckingham, E., 1914. On physically similar systems; illustration of the the use of dimensional equations. Phys. Rev. 2. Ser. 4, 345–376.

Carlier, J., Stanislas, M., 2005. Experimental study of eddy structures in a turbulent boundary layer using particle image velocimetry. J. Fluid Mech. 535, 143–188.

Davidson, P.A., 2004. Turbulence: An Introduction for Scientists and Engineers. Oxford University Press, London, United Kingdom.

DeGraaff, D.B., Eaton, J.K., 2000. Reynolds-number scaling of the flat-plate turbulent boundary layer. J. Fluid Mech. 422, 319–346.

Durst, F., Jovanović, J., Sender, J., 1995. LDA measurements in the near-wall region of a turbulent pipe flow. J. Fluid Mech. 295, 305–335.

Fischer, M., 1999. Turbulente wandgebundene Strömungen bei kleinen Reynoldszahlen. Ph.D. Thesis, University Erlangen Nürnberg.

Fernholz, H.H., Finley, P.J., 1996. The incompressible zero-pressure-gradient turbulent boundary layer: an assessment of the data. Prog. Aerospace Sci. 32, 245–311.

Gad-el-Hak, M., Bandyopadhyay, P.R., 1994. Reynolds number effects in wall-bounded turbulent flow. Appl. Mech. Rev. 47, 307–364.

Gersten, K., Herwig, H., 1992. Strömungsmechanik Fundamentals and Advances in the Engineering Science. Verlag Vieweg.

Hoyas, S., Jiménez, J., 2006. Scaling of velocity fluctuations in turbulent channels up to $Re = 2000$. Phys. Fluids 18, 011702.

Hoyas, S., Jiménez, J., 2005. Scaling of velocity fluctuations in turbulent channels up to $Re = 2003$. Center for Turbulence Research Annual Research Briefs. pp. 51–356.

Hu, Z.W., Morfey, C.L., Sandham, N.D., 2006. Wall pressure and shear stress spectra from direct simulations of channel flow. AIAA J. 44, 1541–1549.

Hussain, A.K.M.F., 1986. Coherent structures and turbulence. J. Fluid Mech. 173, 303–356.

Hutchins, N., Marusic, I., 2007. Evidence of very long meandering features in the logarithmic region of turbulent boundary layers. J. Fluid Mech. 579, 1–28.

Iwamoto, K., Suzuki, Y., Kasagi, N., 2002. Reynolds number effect on wall turbulence: toward effective feedback control. J. Heat Fluid Flow 23, 678–689.

Jiménez, J., Hoyas, S., 2008. Turbulent fluctuations above the buffer layer in wall-bounded flows. J. Fluid Mech. 611, 215–235.

Karlsson, R.I., Johansson, A.V., 1986. Measurement in a plane wall jet in a large enclosure. In: Proc. Sixth Int. Symp. on LDA, Lisbon Portugal.

Khujadze, G., Oberlack, M., 2007. New scaling laws in ZPG turbulent boundary layer flow. In: Fifth International Symposiumon Turbulence and Shear Flow Phenomena, Munich Germany.

Kim, J., Moin, P., Moser, R., 1987. Turbulence statistics in a fully developed channel flow at low Reynolds number. J. Fluid Mech. 177, 133–166.

Klewicki, J.C., Murray, J.A., Falco, R.E., 1994. Vortical motion contributions to stress transport in turbulent boundary layer. Phys. Fluids 6, 277–286.

Laadhari, F., 2002. On the evolution of maximum turbulent kinetic energy production in a channel flow. Phys. Fluids 14, L65–L68.

Ligrani, P.M., Bradshaw, P., 1987. Spatial resolution and measurement of turbulence in the viscous sublayer using subminiature hot-wire probes. Exp. Fluid 5, 407–417.

Long, R.R., Chen, T.-C., 1981. Experimental evidence for the existence of the 'mesolayer' in turbulent systems. J. Fluid Mech. 105, 19–59.

Marusic, I., Kunkel, G.J., 2003. Streamwise turbulence intensity for flat-plate boundary layers. Phys. Fluids 15, 2461–2464.

McKeon, B.J., Li, J., Jiang, W., Morrison, J.F., Smits, A.J., 2004. Further observations on the mean velocity distribution in fully developed pipe flow. J. Fluid Mech. 501, 135–147.

Metzger, M.M., Klewicki, J.C., 2001. A comparative study of near-wall turbulence in high and low Reynolds number boundary layer. Phys. Fluids 13, 692–701.

Metzger, M.M., 2006. Length and time scales of the near-surface axial velocity in a high Reynolds number turbulent boundary layer. Heat Fluid Flow 27, 534–541.

Mochizuki, S., Nieuwstadt, F.T.M., 1996. Reynolds-number-dependence of the maximum in the streamwise velocity fluctuations in wall turbulence. Exp. Fluids 21, 218–226.

Monin, A.S., Yaglom, Y.M., 1971. Statistical fluid mechanics: mechanics of turbulence. In: Lumley, J.L. (Ed.), English Translation, vol. 2. MIT Press, Cambridge, Massachusetts.

Morrison, J.F., 2009. Private communication.

Morrison, J.F., 2007. The interaction between inner and outer regions of turbulent wall-bounded flow. Philos. Trans. R. Soc. A 365, 683–698.

Morrison, J.F., McKeon, B.J., Jiang, W., Smits, A.J., 2004. Scaling of the streamwise velocity component in turbulent pipe flow. J. Fluid Mech. 508, 99–131.

Moser, R.D., Kim, J., Mansour, N.N., 1999. Direct numerical simulation of turbulent channel flow up to $Re_\tau = 590$. Phys. Fluids 4, 943–945.

Nagano, Y., Tagawa, M., Tsuji, T., 1992. Effects on adverse pressure gradient on mean flow and turbulence statistics in a boundary layer. In: Durst, F., Friedrich, R., Launder, B.E., Schmidt, F.W., Schuhmann, U., Whitelaw, J.H. (Eds.), Turbulent Shear Flow, vol. 8. Springer, Berlin, pp. 7–21.

Nickels, T.B., Marusic, I., Hafez, S., Hutchins, N., Chong, M.S., 2007. Some predictions of the attached eddy model for a high Reynolds number boundary layer. Philos. Trans. R. Soc. A 365, 807–822.

Nockemann, M., Abstiens, R., Schober, M., Bruns, J., Eckert, D., 1994. Messungen in einer turbulenten Wandgrenzschicht bei grossen Reynolds-Zahlen im Deutsch-Niederländischen Windkanal Messbericht. In: Krause, E. (Eds.), Abhandlungen aus dem Aerodynamischen Institut der RWTH Aachen.

Osaka, H., Kameda, T., Mochizuki, S., 1998. Re-examination of the Reynolds number effect on the mean flow quantities in a smooth wall turbulent boundary layer. JSME Int. J. 41, 123–129.

Panton, R., 2007. Composite expansion of active and inactive motions of the streamwise Reynolds stress. In: 5^{th} Int. Sym. Turbulence and Shear Flow Phenomena München Germany. pp. 437–441.

Priyadarshana, P.J.A., Klewicki, J.C., 2004. Study of the motions contributing to the Reynolds stress in high and low Reynolds number turbulent boundary layers. Phys. Fluids 16, 4586–4600.

Priyadarshana, P.J.A., Klewicki, J.C., Treat, S., Foss, J.F., 2007. Statistical structure of turbulent-boundary layer velocity–vorticity products at high and low Reynolds number. J. Fluid Mech. 570, 307–346.

Purtell, P., Klebanoff, P., Buckley, F., 1981. Turbulent boundary layer at low Reynolds number. Phys. Fluids 24, 802–811.

Rao, K.N., Narasimha, R., Badri Narayanan, M.A., 1971. The 'bursting' phenomenon in a turbulent boundary layer. J. Fluid Mech. 48, 339–352.

Schlatter, P., Örlü, R., Li, Q., Brethouwer, G., Fransson, J.H.M., Johansson, A.V., Alfredsson, P.H., Henningson, D.S., 2009. Turbulent boundary layers up to $Re_\theta = 2500$ studied through simulation and experiment. Phys. Fluids 21, 051702.

Spalart, P., 1988. Direct simulation of turbulent boundary layer up to $Re_\theta = 1410$. J. Fluid Mech. 187, 61–98.

Sreenivasan, K.R., 1989. The turbulent boundary layer. In: Gad-el-Hak, M. (Ed.), Frontiers in Experimental Fluid Mechanics. Springer-Verlag.

Sreenivasan, K.R., Sahay, A., 1997. The persistence of viscous effects in the overlap region, and the mean velocity in turbulent pipe and channel flows. In: Panton, R. (Ed.), Self-Sustaining Mechanisms of Wall Turbulence. Computational Mechanics Publications, Southampton, United Kingdom.

Stanislas, M., Perret, L., Foucaut, J.-M., 2008. Vortical structures in the turbulent boundary layer: a possible route to a universal representation. J. Fluid Mech. 602, 327–382.

Townsend, A.A., 1976. The Structure of Turbulent Shear Flow. Cambridge University Press.

Tsuji, Y., Fransson, J.H.M., Alfredsson, P.H., Johansson, A.V., 2007. Pressure statistics and their scaling in high-Reynolds-number turbulent boundary layers. J. Fluid Mech. 585, 1–40.

Tsukahara, T., Seki, Y., Kawamura, H., Tochio, D., 2002. DNS of turbulent channel flow at very low Reynolds numbers. In: Proc. Fourth Int. Symp. Turbulence and Shear Flow Phenomena, Williamsburg, USA, pp. 935–940.

Ueda, H., Hinze, J.O., 1975. Fine-structure turbulence in the wall region of a turbulent boundary layer. J. Fluid Mech. 67, 125–143.

Wagner, C., Hüttel, T.J., Friedrich, R., 2001. Low-Reynolds-number effects derived from direct numerical simulations of turbulent pipe flow. Comput. Fluids 30, 581–590.

Wu, X., Moin, P., 2008. A direct numerical simulation on the mean velocity characteristics in turbulent pipe flow. J. Fluid Mech. 608, 81–112.

Zanoun, E.-S., 2003. Answers to some open questions in wall-bounded laminar and turbulent shear flows. Ph.D. Thesis, University Erlangen Nürnberg.